Offline laser power modulation in LPBF additive manufacturing including kinematic and technological constraints

Kamel Ettaieb, Kevin Godineau, Sylvain Lavernhe, Christophe Tournier

▶ **To cite this version:**

Kamel Ettaieb, Kevin Godineau, Sylvain Lavernhe, Christophe Tournier. Offline laser power modulation in LPBF additive manufacturing including kinematic and technological constraints. Rapid Prototyping Journal, 2022, 29 (1), pp.80-91. ⟨10.1108/RPJ-02-2022-0062⟩. ⟨hal-03744945⟩

HAL Id: hal-03744945

https://hal.science/hal-03744945v1

Submitted on 3 Aug 2022

HAL is a multi-disciplinary open access archive for the deposit and dissemination of scientific research documents, whether they are published or not. The documents may come from teaching and research institutions in France or abroad, or from public or private research centers.

L'archive ouverte pluridisciplinaire **HAL**, est destinée au dépôt et à la diffusion de documents scientifiques de niveau recherche, publiés ou non, émanant des établissements d'enseignement et de recherche français ou étrangers, des laboratoires publics ou privés.

HAL Authorization

Offline laser power modulation in LPBF additive manufacturing including kinematic and technological constraints

Kamel Ettaieb, Kevin Godineau, Sylvain Lavernhe, Christophe Tournier

Université Paris-Saclay, ENS Paris-Saclay, Institut Farman (FR3311), LURPA

91190 Gif-sur-Yvette, France

Abstract

Purpose

In laser power bed fusion (LPBF), the process and operating parameters influence the mechanical and geometrical characteristics of manufactured parts. Therefore, the optimization and control of these parameters are mandatory to improve the quality of the produced parts. During manufacturing, the process parameters are usually constant regardless of the part size or the built layer. With such settings, the manufacturing process may lead to inhomogeneous thermal behavior and local overheating areas, affecting part quality. The aim of this work is to take advantage of an analytical thermal model to modulate the laser power upstream of manufacturing.

Design/methodology/approach

The approach follows two steps: the first step involves calculating the preheating temperature at the considered point and the second step determines the power modulation of the laser to reach the desired temperature at this point.

Findings

Numerical investigations on several use cases show the effectiveness of the method for controlling the overheated areas and to homogenize the simulated temperature distribution.

Originality/value

The specificity of this model lies in its ability to directly calculate the amount of energy to supply without iterative calculations. Furthermore, to be as close as possible to the technology used in LPBF machines, the kinematic behavior of the scanning head and the laser response time are also integrated into the calculation.

Keywords

LPBF; power modulation; scanning path; thermal modeling ; kinematical behavior

1 Introduction

Laser Power Bed Fusion allows producing three-dimensional parts layer by layer from 3D model data. This technology involves locally melting a layer of powder (between 20 to 100 μm) using a laser beam. LPBF has undergone a rapid development in the industrial sector over the last ten years. Nevertheless, it still suffers from several quality problems. Indeed, the LPBF process has many input parameters, which influence the quality of the produced parts (Zhang et al., 2017). Among these, the most important are the laser power P, scanning speed V, hatching distance h, layer thickness e and scanning path. These parameters directly influence the temperature and thus the stability of the melt pool during the manufacturing process. A melt pool is stable when it maintains constant dimensions and does not exhibit any disturbance or convective movement that affects the quality of the part. This allows homogeneous and flawless beads to be obtained. An incorrect parameter setting causes an unstable melt pool. In this case, the dimensions of the molten area change during the manufacturing process and the melt pool shows a disturbed hydrodynamic behavior (Marangoni effect, splashing, etc.). The synthesis presented in the review paper provided by Mani et al. (Mani et al., 2015) shows the correlation between the process parameters, the temperature level, the size of the melt pool and the quality of the produced parts.

The complete melting of the material requires to provide sufficient energy, characterized by the volumetric energy density E supplied to the powder bed and function of power, scanning speed, layer thickness and hatching distance (Thijs et al., 2010). In general, the combinations of speed and power lead to identify different operating modes that can take place during the manufacturing process (Oliveira et al., 2020) (Figure 1).

The first operating mode corresponds to the process window in which the manufacturing strategy is optimal in terms of power and scanning speed. The laser energy is efficiently absorbed by the powder, creating a melt pool of sufficient depth to ensure the junction of the material with the previous layer, while avoiding excessive remelting. This leads to a fully dense part with a minimum of defects (Bertoli et al., 2017).

The second operating mode is an unstable mode that occurs when the power is high and the laser speed is low, leading to the well-known ”keyhole” effect (Gong et al., 2014). The depth of the melt pool becomes important and the temperature reaches the vaporization temperature of the material. These phenomena cause the formation of spatters (Dai et al., 2015), generates spherical porosities originating from gas bubbles trapped in the melt pool (Gong et al., 2015) and important thermal gradients which in turn lead to residual stresses (Mugwagwa et al., 2018).

The third operating mode occurs when the power is low for a given speed. In this case, the depth of the melted area does not allow the full melting of the powder layer and the junction between layers (Coeck et al., 2019). This leads to a lack of fusion, which in turn causes excessive porosity and delamination. These types of defects have a significant influence on the mechanical properties of LPBF parts, in particular, the fatigue resistance (Zhang et al., 2017) as they can be the cause of the appearance of cracks in the part.

The fourth operating mode takes place when the scanning speed is high for a given power. In this case

the behavior of the melt pool becomes unstable and a beading effect, which is known as ”balling up”, is created (Bertoli et al., 2017). Indeed, the delivered energy is sufficient to melt the powder and the high speed of the laser generates a flow from the center and the front edge of the melt pool to its back. This phenomenon leads to the irregular beads and humping formation which influence the surface quality.

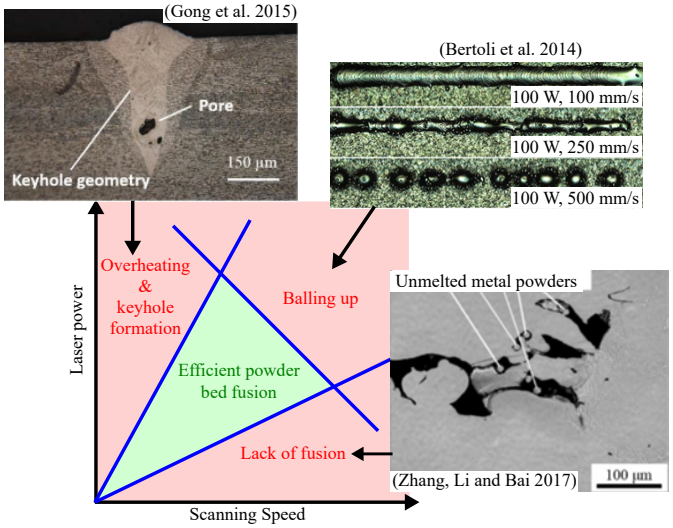

Figure 1: Stable and unstable manufacturing states with laser power and scanning speed diagram

In order to limit the defects presented above, it is necessary to identify for each material a set of parameters included in the stable process window and thus define the dedicated manufacturing strategy. This identification is generally the result of experimental tests (Muta et al., 2018) or numerical simulations using thermomechanical models (Nakapkin et al., 2019).

Some machine manufacturers adapt the operating parameters to the part geometry, for example for overhanging areas or thin structures. However, most of the time the operating parameters remain constant during manufacturing, regardless of the scannning path. On the one hand, the geometrical characteristics of the manufactured part such as sharp angles impact the thermal behavior and generate overheated areas. On the other hand, the scanning path influences the temperature and the size of the melt pool during the manufacturing process. Indeed, the laser path plays a major role in heat dissipation, and each path generates a specific thermal behavior during melting.

In the literature, many research works are focused on real-time control of additive manufacturing processes to improve part quality. Kruth et al. (Kruth et al., 2007) developed a feedback system that adjusts the laser power to keep the melt surface constant throughout the manufacturing process. The control is done using two sensors, a CMOS camera and a photodiode coaxially mounted with the laser beam. Real-time power adjustment allows the control of the melt pool size and thus improve the geometrical quality and decreases the surface roughness of the manufactured part. Modulation of process parameters during manufacturing has also been investigated by the NIST (Lane et al., 2016). They developed an additive manufacturing testbed to control power and scanning speed in order to stabilize the size of the melt pool along the path. Experimental results showed the importance of the method to homogenize the temperature distribution and to improve the melting quality (Yeung et al., 2018). They also proposed an

algorithm for controlling laser power based on a Geometric Conductance Factor (GCF) estimated according to the characteristics of the solid or powder material near the melt pool (Yeung et al., 2019). It allows the reduction of the laser power in the vicinity of less conductive powder, near edges within a layer and above overhangs in lower layers. The laser power adjustment reduces the melt pool variability and thus improves the surface quality of the produced parts. Nevertheless, the GCF controller is calculated on the geometric characteristics of the part and is not directly tied to a thermal model and to heat absorption and transfer during the LPBF process. Tapia and Elwany (Tapia et al., 2014) reviewed the technologies used for process monitoring and control of metal-based additive manufacturing showing the diversity of the proposed solutions. Nevertheless, most of them consist in controlling the melt pool size and not the temperature level. This is mainly related to hardware issues, especially measurement sensors. Indeed, the developed monitoring systems are promising, but the modulation of the process parameters in real time remains limited and difficult to integrate in industrial machines due to the complexity and the speed of the manufacturing process.

In this context, a few approaches propose to modulate the parameters upstream of the manufacturing process through numerical simulations. A solution was proposed by Beraud and al. within the context of the EBM process (Beraud et al., 2014). First, a thermal simulation allows for generating temperature charts with different parameters settings. Secondly, these charts are used to modulate the energy brought to the material in order to control the maximum temperature during the manufacturing process. Forslund et al. (Forslund et al., 2021) used an analytical solution of the heat equation to optimize the speed and diameter of the laser beam. The simulations showed that the modulation of these parameters allows obtaining homogeneous temperature mappings and to maintain a constant area of the melt pool throughout the path. The main drawback of this approach is the iterative calculation. At each moment, the optimal values of scanning speed and laser beam size are computed by iterative testing which is time consuming and not suitable for very high frequency control.

In LPBF process, many simulation models have been developed (Kushan et al., 2018). However, their complexity remains an obstacle that limits their use in process parameters modulation. Furthermore, it is difficult to predict the time and location on the surface where the temperature reaches its maximum value. The position where the temperature is maximum evolves according to the geometry of the path and to the diffusion of the thermal flux resulting from the laser path. For this reason, the prediction of the temperature using the classical simulation methods, as Finite Element Method (FEM) or Finite Difference Method (FDM), requires iterative calculations. These models are therefore once again time consuming and can hardly be considered to simulate the temperature for a part, on a local scale, taking into account the displacement of the laser.

Moreover, it is also necessary to consider the real trajectory of the laser in the working plane and not only the programmed trajectory to modulate the power along the scanning path. Indeed, the requirements in terms of scanning speed are such that the dynamic behavior of the galvanometers does not allow the execution of the trajectories without contour error and speed slowdowns, in particular when passing tangential discontinuities. Thus, in order to integrate this behavior in the simulation of the local modulation of the laser power, kinematic measurements have been carried out on a test bench which operates industrial scanning heads and in particular the Cambridge Technology Lightning II head implemented on the FormUp 350 machine.

In this context, this paper presents a method to modulate the laser power in order to control the temperature at the laser beam center for a given path. The novelty lies in the use of an efficient thermal

simulation which does not require iterative computations and also integrates the kinematics of the galvanometric head control in the calculation. The aim is to take advantage of the preheating temperature at each point along the path and to modulate the power to ensure a constant temperature when the laser irradiates this point. The method makes it possible to determine the desired quantity of energy upstream to obtain a constant temperature in a fast way.

The rest of this paper is organized as follows: the thermal model and the simulation strategy are reminded in the second section. The third section is dedicated to the power modulation approach and its application to case studies. Finally, the paper ends with a conclusion and some perspectives.

2 Thermal modeling

2.1 Governing equations

Laser powder bed fusion is a fast melting and solidification process. The temperature varies greatly according to the time and the space with the displacement of the heat source. In this sense, the macroscopic temperature field analysis of this process is a typical problem of non-linear transient heat conduction. In a domain Ω, the spatial and temporal distribution of the temperature field is defined by the heat equation (1).

$$\rho C \frac{\partial T}{\partial t} = \lambda \nabla^2 T + Q \tag{1}$$

where ρ is the material density [kg.m^{-3}], C is the specific heat capacity [J.kg^{-1}.K^{-1}], T is the temperature [K], λ is the thermal conductivity [W.m^{-1}.K^{-1}], and Q is the heat source generated by the laser [W.m^{-3}]. Considering n as the normal vector to the interface, the boundary condition at the top surface of the powder is written as follows [Equation (2)]:

$$-\lambda \frac{\partial T}{\partial n} = q - q_c - q_r \tag{2}$$

where q is the laser surface flux [W.m^{-2}], q_c is the heat lost by convection [W.m^{-2}] and q_r is the heat lost by radiation [W.m^{-2}]. The powder bed is heated to a preheating temperature T_0 at $t = 0$.

In this study, the following assumptions are adopted:

1. The energy distribution is considered as Gaussian.
2. The conductivity λ and the absorptivity A parameters are those of the consolidated material which is common hypothesis in LPBF (Forslund et al., 2019).
3. Physical properties of materials are considered to be independent of the temperature.
4. Radiation q_r and convection q_c losses are considered to be null.
5. Phase change and the latent heat are not taken into account in the simulation.

In this context, the thermal problem of powder melting is reduced to a conduction problem after the interaction between the laser and the material. An explicit formulation of the evolution of the temperature in the part over time is proposed.

2.2 Thermal modeling using the Flash method

As detailed in (Ettaieb et al., 2020)), an analytical thermal simulation based on the Flash method has been proposed and validated by comparison with a reference FEM software and experimental results within a Ti6Al4V test case. Indeed, the Flash method is commonly used to measure the thermal diffusivity of materials. The principle consists in loading a plate of thickness L and radially semi-infinite on its front surface by impulse excitation $\delta(t)$ (Dirac function), which has a Gaussian distribution of radius R. Considering z as the downward vertical axis, r the radial direction, $z = 0$ represents the top surface and $r = 0$ the center of the laser beam. Then, its impulse response in temperature is measured on the irradiated surface. The sample is supposed to be homogeneous, isotropic, and opaque. The mathematical modeling of these phenomena leads to the following differential equations (Cernuschi et al., 2001):

$$\nabla^2 T(r,z,t) = \frac{1}{\alpha} \cdot \frac{\partial T(r,z,t)}{\partial t} \tag{3}$$

where α is the thermal diffusivity [$\mathrm{m}^2.\mathrm{s}^{-1}$]. For the top surface ($z = 0$):

$$-\lambda \frac{\partial T(r,z=0,t)}{\partial z} = \frac{2AQ_l}{\pi R^2} \cdot e^{\frac{-2r^2}{R^2}} \delta(t) \tag{4}$$

where A is the absorptivity of the material, and Q_l is the laser energy [J]. On the opposite surface of the plate $z = L$, a constant heat flux is defined as follows (Eq. (5)):

$$-\lambda \frac{\partial T(r,z=L,t)}{\partial z} = 0 \tag{5}$$

The laser energy is calculated as follows [Equation (6)]:

$$Q_l = P \cdot \Delta t \tag{6}$$

where Δt is the elementary duration of the laser emission.

The analytical resolution of Eq. (3) leads to the calculation of the thermal effect of a flash (T_f), which is written as follows equation (7)):

$$T_f(r,z,t) = \frac{2AQ_l}{\varepsilon\sqrt{\pi^3 t}} \cdot \frac{1}{R^2 + 8\alpha t} \cdot e^{\frac{-2r^2}{R^2+8\alpha t}} \cdot \sum_{n=-\infty}^{\infty} e^{\frac{-[(n-1)L+\frac{z}{2}]^2}{\alpha t}} \tag{7}$$

where ε is the thermal effusivity [$\mathrm{J.K}^{-1}.\mathrm{m}^{-2}.\mathrm{s}^{-\frac{1}{2}}$], which is calculated as a function of the other thermal parameters of the material [Equation (8)]:

$$\varepsilon = \sqrt{\lambda \cdot \rho \cdot C} \tag{8}$$

For $z = 0$ and large values of limit n, the value of the series is tend to 1. Consequently, it is possible in this case to neglect this term in the expression of the temperature. The temperature response given by the Flash method at the surface ($z = 0$) can be expressed by equation (9):

$$T_f(r,0,t) = \frac{2AQ_l}{\varepsilon\sqrt{\pi^3 t}} \cdot \frac{1}{R^2 + 8\alpha t} \cdot e^{\frac{-2r^2}{R^2+8\alpha t}} \tag{9}$$

The thermal effect of flash T_f can be considered as the impulse response of the part due to the laser emission on the surface. Thus, during LPBF process, the irradiation of the laser on the powder according to the scanning path with a given speed can be modeled as a succession of pulses. Therefore, the global temperature response T_g at instant t and on each point of the part defined by coordinates (x,y,z) is the cumulative sum of the impulse responses along the path up to that moment. Considering the preheating temperature of powder T_0, the global temperature T_g at each point (x,y,z) according to time t is expressed by equation (10):

$$T_g(x,y,z,t) = T_0 + \sum_{i=0}^{n} T_{fi}(r_i,z,t-i.\Delta t) \tag{10}$$

$$\text{with } \begin{cases} n = \lfloor \frac{t}{\Delta t} \rfloor \\ r_i = \sqrt{(x-x_i)^2+(y-y_i)^2} \end{cases}$$

where r_i represents the distance between each point of the layer at the top surface (x,y) and the flash center point (x_i,y_i) at instant $i\Delta t$.

As one can see, the explicit formulation of temperature is written as functions of process parameters. Therefore, it is possible to use the model to control temperature by modifying the parameters such as the laser power or the scanning speed. This study focuses on the approach of temperature control at the center of the laser beam by modulating the power of along the path.

3 Power modulation

3.1 Methodology

This section presents the proposed methodology to control the temperature at the center of the laser beam. Power modulation with the Flash method consists in determining the elementary flash to be applied at each point of the considered path in order to obtain the desired temperature value. The principle is based on four steps:

1. Calculate the local preheating temperature T_p due to the heat brought by the laser before it reaches the considered point (x_n,y_n) along the trajectory. The preheating temperature is defined as follows [Equation (11)]:

$$T_p(x_n,y_n,0,n\Delta t) = T_g(x_n,y_n,0,n\Delta t - \delta t) \tag{11}$$

$$\text{with } \delta t = 0^+ \text{ and } n \in \mathbb{N}$$

2. Calculate the temperature $T_f(0,0,t_0)$ at the center of the elementary flash to be generated at the considered point of the path (x_n,y_n) and at the instant $n\Delta t$ of the laser passage on this point. T_f is the difference between the target temperature T_{target} and the preheating temperature T_p according to the following formula [Equation (12)]:

$$T_f(0,0,t_0) = T_{target} - T_p(x_n, y_n, 0, n\Delta t) \tag{12}$$

with t_0 is the temporal local origin of the elementary flash. It represents the lower bound of the validity domain of the model (Cernuschi et al., 2001).

3. Calculate the necessary laser energy $Q_l(n\Delta t)$ to obtain the generated temperature T_f by the flash at the center of the laser beam, at instant $n\Delta t$. It is calculated from Eq. (9) as a function of $T_f(0,0,t_0)$ (Eq. (13)):

$$Q_l(n\Delta t) = \frac{\varepsilon\sqrt{\pi^3 t_0}\cdot(R^2 + 8\alpha t_0)}{2A}\cdot T_f(0,0,t_0) \tag{13}$$

Thus, the delivered power $P(n\Delta t)$ by the laser is written as a function of the laser energy $Q_l(n\Delta t)$ and the temporal step Δt according to the following equation (14):

$$P(n\Delta t) = \frac{Q_l(n\Delta t)}{\Delta t} \tag{14}$$

The power modulation must respect the constraints imposed by the LPBF process. The power and scanning speed values must be within the stable operating window. For a given scanning speed, the value of the power in the operating window is bounded by two threshold values $P_{w_{min}}$ and $P_{w_{max}}$ which represent the minimum power and the maximum power respectively. The nominal power P_n is defined as the center of the power range.

Moreover, the power modulation must respect the technological characteristics of the laser which are its minimum power value $P_{l_{min}}$ which is generally equal to 0, its maximum value $P_{l_{max}}$ and its response time. The overlapping between the power range given by the stable operating window $[P_{w_{min}}, P_{w_{max}}]$ and the power range given by the laser capacity $[P_{l_{min}}, P_{l_{max}}]$ constructs the final admissible range of the modulation power $[P_{min}, P_{max}]$ [Equation (15)] with:

$$\begin{cases} P_{min} = max(P_{w_{min}}, P_{l_{min}}) \\ P_{max} = min(P_{w_{max}}, P_{l_{max}}) \end{cases} \tag{15}$$

Thereby, at each instant $n\Delta t$, the power set point value is bounded by the technological constraints [Equation (16)]:

$$P(n\Delta t) = \begin{cases} P(n\Delta t), & \text{if } P(n\Delta t) \subset [P_{min}, P_{max}] \\ P_{min}, & \text{if } P(n\Delta t) < P_{min} \\ P_{max}, & \text{if } P(n\Delta t) > P_{max} \end{cases} \tag{16}$$

On the other hand, at each instant, the power setpoint value may not be achievable with the actual system. In general, the behavior of the laser during its ignition can be considered as a first order system. Therefore, at a given input excitation, the system goes through a transient regime characterized by the time constant τ [μs] before reaching a steady-state regime. The simulation must

integrate this behavior of the laser response in order to faithfully respect reality.

4. Generate a flash with the previously calculated power setpoint which leads to get closer to the target temperature at the considered point of the scanning path.

The methodology of power modulation, for a given scanning path, is summarized in the diagram Figure 2.

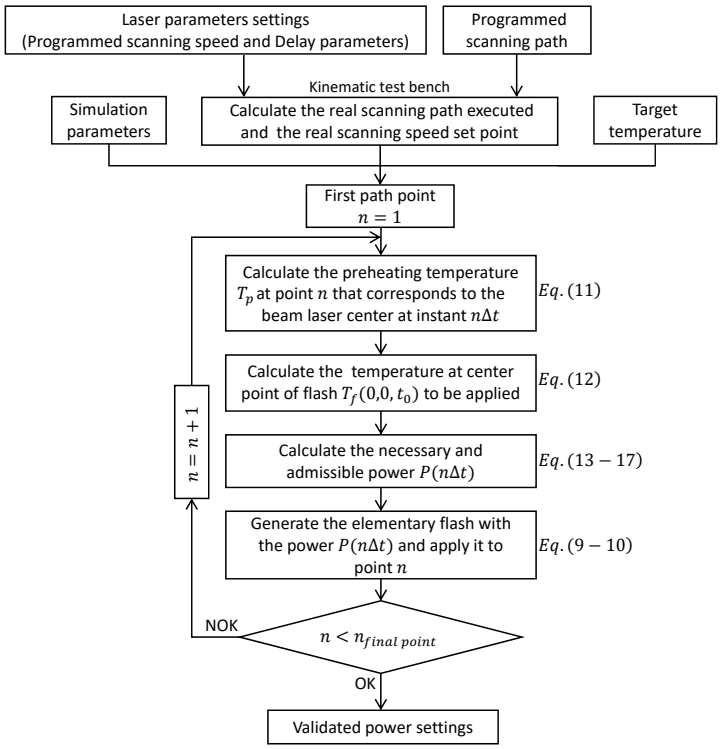

Figure 2: Power modulation methodology

3.2 Kinematic concerns

In order to integrate the kinematic behavior of the real machine in the offline power modulation, an experimental bench equipped with several scanning heads is used Figure 3 to identify the kinematic behavior along the scanning trajectory according to scanning parameters. The card that drives the two galvanometers X and Y of the considered scanning head also records their angular positions along the programmed trajectory, which makes it possible to rebuild the trajectory actually followed by using the direct kinematics (Godineau et al., 2019) and to calculate the reached speeds by finite difference. The kinematic analyses presented in the following case studies is purely experimental. The scanning paths of the tests cases are monitored either on the test bench or directly on the FormUp 350 machine.

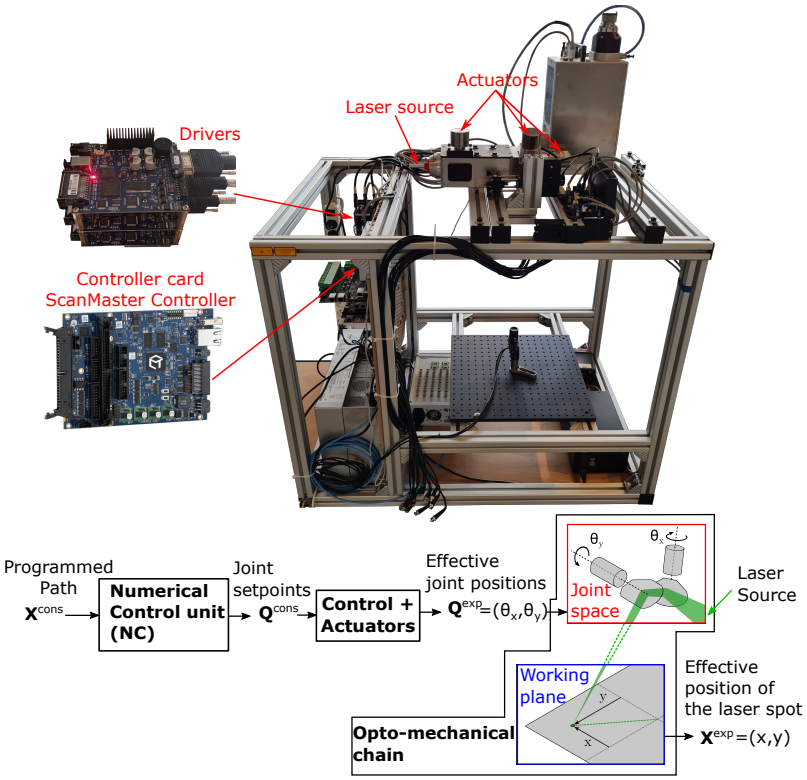

Figure 3: Kinematic test bench of scanning heads and communication architecture

3.3 Case studies

3.3.1 Power modulation in the case of discontinuous zigzag path

To illustrate the relevance of the proposed approach, a zigzag path is tested in the case of a small parallelepipedic part (Figure 4) made of titanium alloy (Ti6Al4V). Table 1 lists the process and material parameters. The used parameters in this simulation correspond to those of the machine FormUp 350 which is equipped with a ND:YAG laser which maximum power value $P_{l_{max}}$ is equal to 500 W.

The scanning speed is programmed to 1 $m.s^{-1}$ during melting and to 6 $m.s^{-1}$ during the jumps between paths. However, as discussed in the introduction, one may wonder about the respect of the programmed scanning speed and trajectories. In this case, the markDelay and jumpDelay control parameters are used by the scanning head to round off the trajectory when changing direction and to slow down (Figure 5a):

- markDelay: delay (μs) added at the end of a segment before the jump allowing the mirrors to move to the required position, prior to executing the next mark command
- jumpDelay: delay (μs) added at the end of the jump allowing the mirrors to reach the required scanning speed for accurate marking

It is possible to integrate small additional vectors at each path extremity (Figure 5b) so that the

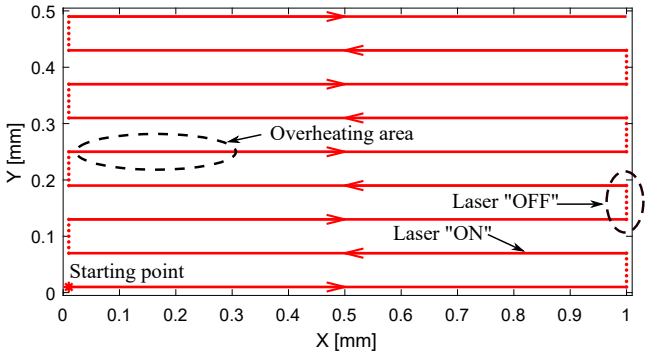

Figure 4: Zigzag scanning path

rounding is done on these vectors without consequences on the part in terms of contour error and scanning speed.

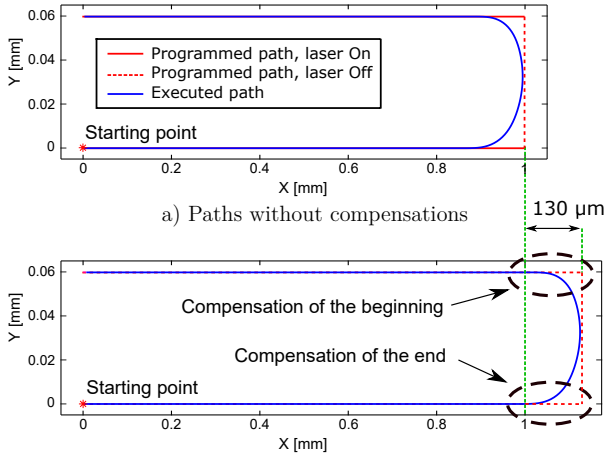

a) Paths without compensations

b) Paths with compensations

Figure 5: Scanning path with or without additional vectors with markDelay $= 120\ \mu s$ and jumpDelay $= 150\ \mu s$

In order to illustrate the effect of adding compensation vectors on the discontinuous scanning path, an experimental study was carried out on the FormUp 350 machine. The principle consists in making a melt track on a substrate along a discontinuous path, with and without compensation vectors. In all cases, the power is set to 25 W and the hatching distance is equal to 60 μm. Figure 6 shows the observation of the tracks obtained using an InfiniteFocus 3D measurement system as well as the programmed and executed paths. The path setpoints are measured directly on the drives of the galvanometric head into the machine. In the case of scanning without added vectors (Figure 6a), the laser is programmed to mark along the X^+ direction until it reaches the vertical line, then jump and finally mark in the opposite X^- direction (blue curve). Measurements show that the laser changes its scanning direction before the end of the programmed vector and starts marking in the second segment behind from the desired position (vertical

green line) leading to a contour error of about 78 μm. In the second case, the same path is programmed by adding two compensation vectors of lengths equal to 130 μm. As shown by the red curve in Figure 6b, the laser reaches the desired position (vertical green line). Nevertheless, an overshoot is observed which is mainly due to the wrong setting of the laser extinction parameter (Laser Off Delay) at the end of the first vector and its ignition (Laser On Delay) at the beginning of the second vector. Finally, for the third and last case (Figure 6c), the compensation vector and the laser extinction and ignition parameters are correctly chosen and the marking path is clearly discontinuous at the specified location.

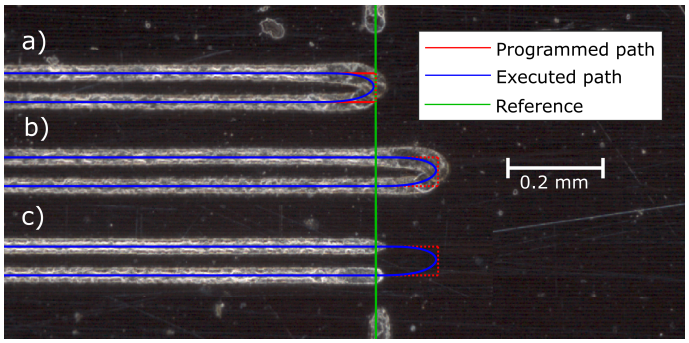

Figure 6: Melt tracks on the substrate, a) without compensation vectors, b) with compensation vectors (130 μm) but wrong laser parameters, c) with compensation vectors (130 μm) and correct laser parameters

Table 1: Simulation parameters

P, laser power	[W]	300
R, effective radius of laser beam	[m]	5.10^{-5}
V, scanning speed	[m s^{-1}]	1
A, absorptivity	[%]	30
λ, thermal conductivity	[W.m^{-1}.K^{-1}]	15
C, specific heat capacity	[J.kg^{-1}.K^{-1}]	800
ρ, density	[kg.m^{-3}]	4420
ε, thermal effusivity	[J.K^{-1}.m^{-2}.$s^{-\frac{1}{2}}$]	7282
T_0, preheating temperature	[K]	293
Δt, temporal step	[s]	1.10^{-5}
τ, laser response time	[μs]	20

The thermal model is implemented in Matlab and all the test cases in this study are run on a laptop computer equipped with an Intel Core i5 6200U @ 2.3 GHz (2 cores) and 8 GB of RAM.

First, the path is simulated with a constant power of 300 W. The computation time is equal to 80 seconds. Figure 7 shows the evolution of the simulated temperatures over time. The red curve represents the evolution of the maximum temperature T_{max}, the blue curve is the temperature at the center point of the laser beam T_{center} and the magenta curve describes the evolution of the preheating temperature T_p at the center point of the laser before the energy is delivered. The black curve represents the power that corresponds to the nominal power given by the process window with a scanning speed of 1 $m.s^{-1}$. Local drops to zero correspond to the laser jump from the end of a segment to the beginning of the next one.

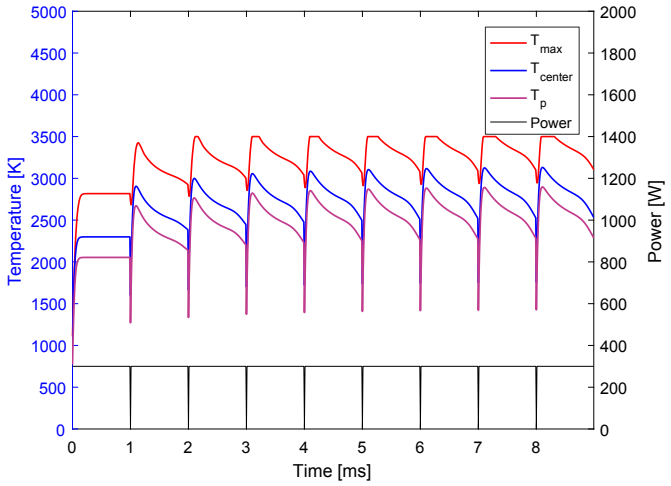

Figure 7: Evolution of temperatures and power over time

One can see that starting from the second line, the temperature profiles undergo large and repetitive fluctuations. At the beginning of each line, the simulated temperatures are low (i.e. preheating due to the heat conduction from previous segment), and then they increase quickly due to the effect of heat accumulation. After that, the temperature values decrease gradually until the end of the line. For example, at the beginning of the fifth line, at 4 ms, the preheating temperature is 1400 K. The temperature at the center and the maximum temperature are equal to 1735 K and 2912 K respectively. Given the fact that the path at the beginning of the next line starts in the opposite direction, it benefits from the radial thermal conduction. Locally, the thermal diffusion increases rapidly the preheating temperature of the rest of the path to reach a value equal to 2810 K within a period of 0.1 ms. Therefore, the temperature at the center and the maximum temperature increase. The maximum central recorded temperature is equal to 3100 K with a total variation of 1365 K and the maximum temperature reaches the vaporization temperature (3500 K), with a total variation equal to 588 K, leading to a heterogeneous temperature map (Figure 8). From a macroscopic point of view, the zigzag path with constant parameters leads to overheating areas when changing the scanning direction.

Fluctuations in the maximum temperature lead to a large variation in the size of the melt pool. Indeed, in the case of the zigzag path, when the laser reaches the end of a line and starts again in the opposite direction, the generated melt pool has a complex shape, the width of which is difficult to calculate. Thus,

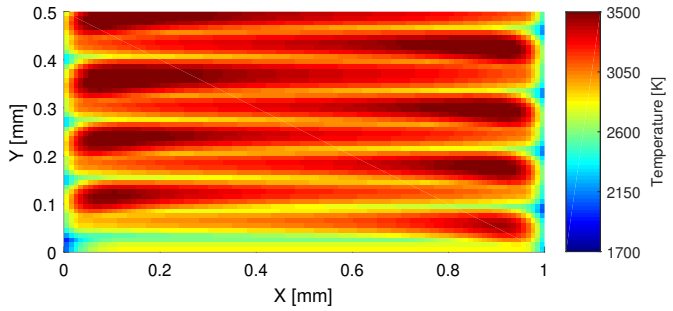

Figure 8: Map of maximum temperature on the surface ($z = 0$)

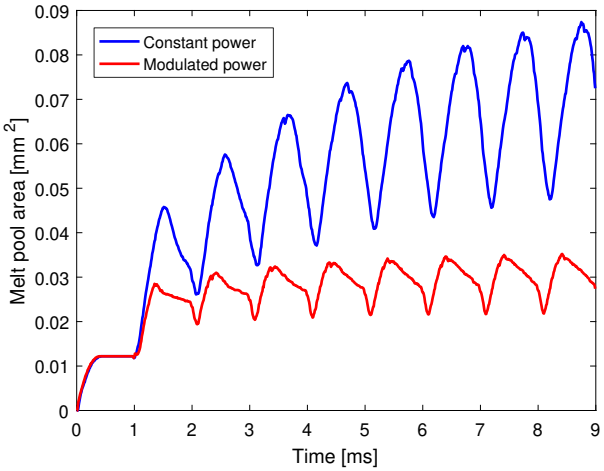

Figure 9: Evolution of the melt pool area with constant and modulated power

in order to characterize the behavior of the melt pool, its surface area has been evaluated. Figure 9 shows the evolution of the melted area over time (blue curve). It can be seen that from the second line (1 ms), the melt pool area varies between 0.012 mm^2 and 0.085 mm^2.

The evolution of the temperature at each point of the path is presented in Figure 10. It is clear that the temperature increases very quickly at the beginning of each line over a portion of 0.1 mm length. Then it decreases as the laser moves forward from the second line. The drop of temperature at the beginning of each line is due to the discontinuity of the zigzag path. Indeed, the heat dissipation in the scanning direction is greater than in the perpendicular direction. In addition, as the maximum temperature is located behind the center of the laser, the maximum width of the heat trail is also located behind the center point of laser-matter interaction. At the end of a line, the laser turns off and moves with rapid velocity to turn on at the beginning of the next line. When the laser arrives at the beginning of the new line, the temperature is yet low because the jump speed of the laser is faster than the speed of heat propagation from previous line. Then, the temperature increases progressively under the radial dissipation of the heat and the thermal flux resulting from the last points of the previous line.

After studying constant power simulations, let us now consider the power modulation simulation.

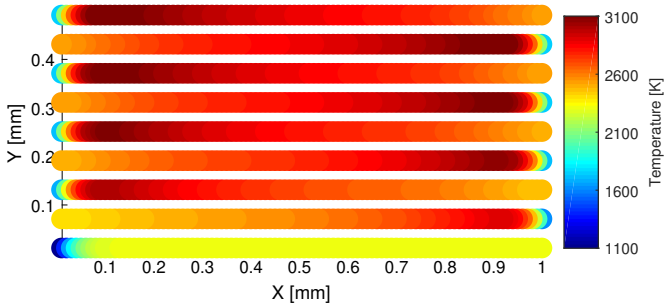

Figure 10: Evolution of temperature at the center point

The target temperature is set to 2300 K allowing the melting of all the powder bed. In order to respect the power limits imposed by the process window of Ti6Al4V and the machine constraints, the admissible power range is set to [100 W; 500 W]. Figure 11 shows the evolution of temperatures with the power modulation. One can see that the method enables to maintain a constant temperature value throughout the path except at the beginning of each line. To maintain this value, the laser power varies from 140 W to 430 W and thus remains within the admissible interval. As for the constant power test, drops in power to zero correspond to the laser jump between two successive scanning vectors.

As one can see in the zoomed area at the very beginning of the fifth segment (Figure 11), at 4 ms, the preheating temperature T_p decreases at the beginning of each segment. Thus, the power rises as quick as possible to increase the temperature at the center point toward the target temperature while being limited by the laser response time (20 μs). Locally, the power reaches a maximum value equal to 430 W and the target temperature at the center point reaches a maximum temperature of 1825 K at the beginning of each segment.

Thereafter, the heat arising from the previous line increases the preheating temperature. As a result, the laser power decreases in order to reduce the laser energy and to ensure the target temperature value at the beam center. Nevertheless, there is not enough time so that the laser reaches a stable state and provides the required theoretical power value. This transient behavior explains the appearance of temperature peaks at the beginning of each segment. Nevertheless, the maximum error recorded is equal to 5% of the target value.

Afterwards, when the laser moves on the segment, the preheating temperature gradually decreases. In order to respect the temperature set points, the power increases slowly until the end of the segment. The temperature control at the center of the laser beam enables to reduce the maximum temperature value and its fluctuations during the manufacturing process (red curve on Figure 11). The maximum values vary between 2600 K and 2800 K which is much lower than the vaporization temperature (3500 K). Figure 12a shows the power setpoints for the whole path. The power value is constant during the first line. From the second line, the power is maximum at the beginning of the segment then decreases to reduce the temperature in the heat accumulation area and then it gradually increases until the end of the segment.

The comparison of the temperature maps in Figure 8 and Figure 12b confirms the efficiency of the power modulation on the thermal behavior. The thermal distribution is more homogeneous than the one obtained with constant process parameters. The minimum temperature measured on the surface is equal to 1900 K, thus higher than the melting temperature.

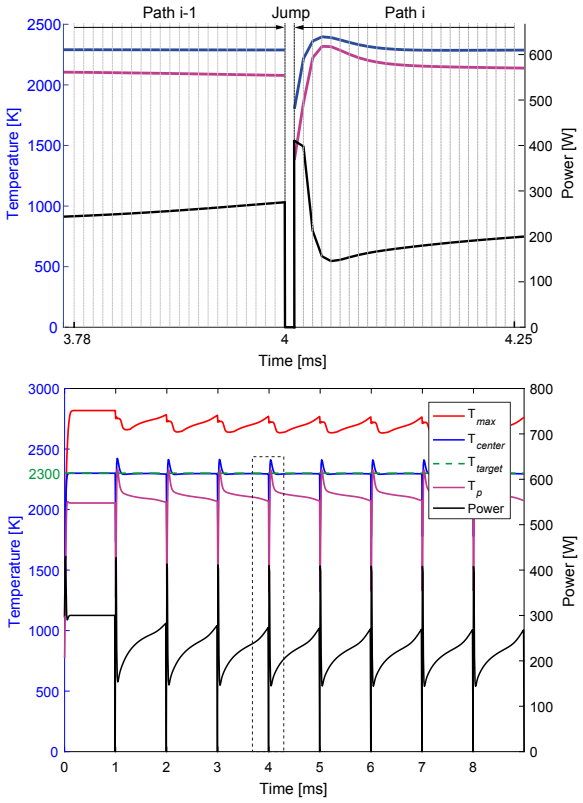

Figure 11: Evolution of temperatures and power over time in the case of a power modulation

In addition, power modulation reduces the size of the melt pool to the minimum required to ensure sufficient overlap between the beads. Its fluctuations are reduced and more stable compared to that generated by the constant power. The area evolves between 0.012 mm^2 and 0.035 mm^2 (red curve on the Figure 9). As mentioned previously, the increase of the melted surface leads to the increase of the surface tension and the appearance of the Marangoni effect (Dai et al., 2015). These phenomena generate splashes and humps that can impact the surface quality and the geometric characteristics of the produced parts (Kruth et al., 2007). In this sense, temperature control during the manufacturing process may avoid or greatly reduce the appearance of these defects.

3.3.2 Power modulation in the case of continuous zigzag path with kinematical constraints

In order to solve the problem of the temperature decrease at the beginning of each segment, it is possible to consider continuous zigzag scanning path allowing a continuous flux of heat upstream of the laser. In this case, the laser remains on all along the scanning path. However, these changes in direction along the scanning path will inevitably cause slowing and rounding. Contrary to the previous case, it is not possible to introduce additional compensation vectors since the laser remains on. In this case, the polyDelay parameter drives the contour error (Figure 13) and slowing down behavior (Figure 14) in the sharp corners. Thus the laser power must be modulated taking into account the effect of the polyDelay

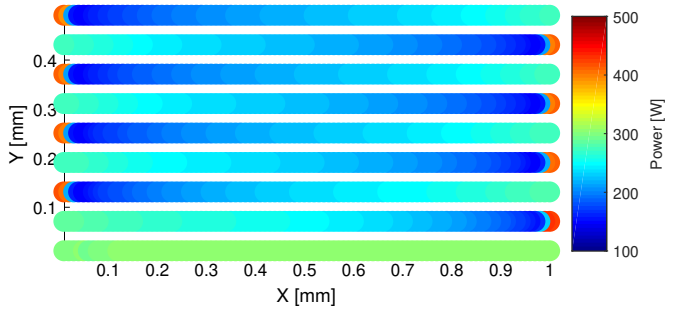

(a) Evolution of power

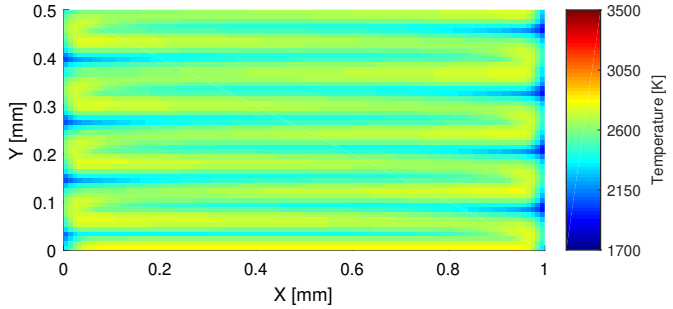

(b) Map of the maximum temperature

Figure 12: Evolution of power and map of maximum temperature for power modulation and discontinuous zigzag path

parameter in terms of geometry and scanning speed.

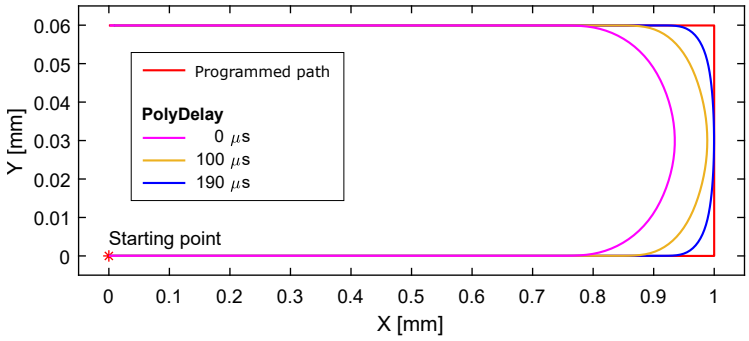

Figure 13: Evolution of rounding effect at sharp corners according to the value of the polyDelay parameter

To illustrate the effect of the polyDelay parameter on the continuous zigzag path, an experimental investigation was performed on the FormUp 350 machine consisting in making a melt tracks on a substrate with two different polyDelay values (0 μs and 190 μs). In this study, the power and the hatching distance are set to 25 W and 60 μm respectively. The observations are presented in Figure 15. As expected, when the polyDelay parameter is equal to zero, the laser does not follow exactly the programmed path (red

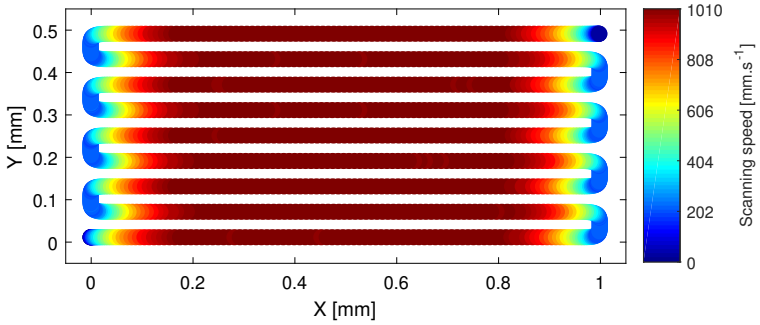

Figure 14: Evolution of scanning speed at sharp corners with the polyDelay parameter equal to 190μs

curve). It changes its scanning direction (blue curve) before reaching the programmed position (vertical green line). The generated maximum contour error is about 70 μm. In addition, a slight increase in the track width is observed with a decrease in the scanning speed when changing direction. When the value of polyDelay is equal to 190 μs (Figure 15b), the executed path is closer to the programmed path. However, the significant decrease in scanning speed further increases the temperature and thus the width of the track in the transition area.

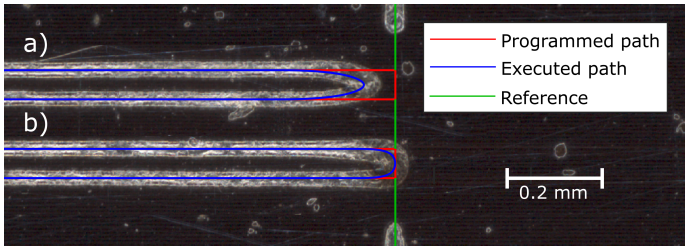

Figure 15: Melt tracks on the substrate, a) polyDelay = 0 μs, b) polyDelay = 190 μs

Figure 16a presents the maximum temperature maps of the scanning paths calculated with a polyDelay equal to 190 μs. The power of the laser is constant and set to 300 W. As shown in figures, the area of overheating at the part extremities are very large. This is due to the decrease of the scanning speed in these areas according to the PolyDelay parameter and, to the local preheating effect generated when changing the scanning direction. The scanning paths calculated with a polyDelay equal to 190 μs is simulated with modulated power and a target temperature at the center of the laser spot equal to 2300 K. The maximum temperature map is presented in Figure 16b. It is clear that the power modulation reduces and eliminates the thermal effects generated by the geometry of this path and the associated kinematical constraints. This results in a more homogeneous maximum temperature map. The maximum temperature doesn't exceed the value of 2830 K.

At last, Figure 17 shows the temperature profiles along the continuous zigzag path. The temperature is almost constant over time. As mentioned above, the small overheating in the center point curve is caused by the laser's response time. The maximum temperature on the path (red curve) varies between 2630 K and 2830 K.

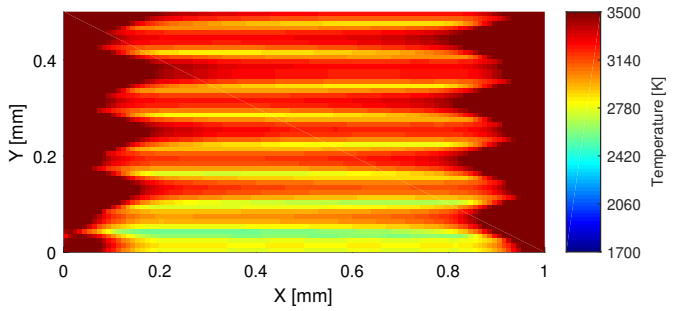

(a) Constant power, $polyDelay = 190\ \mu s$

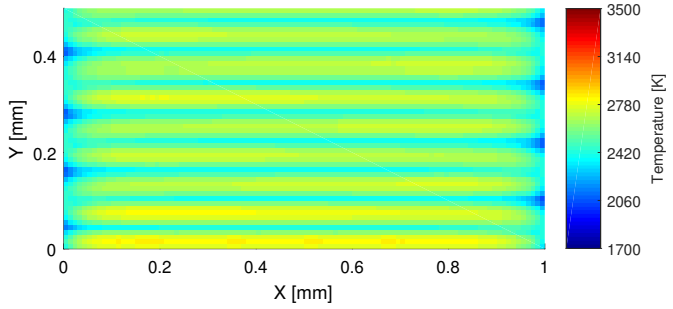

(b) Modulated power, $polyDelay = 190\ \mu s$

Figure 16: Maps of the maximum temperature

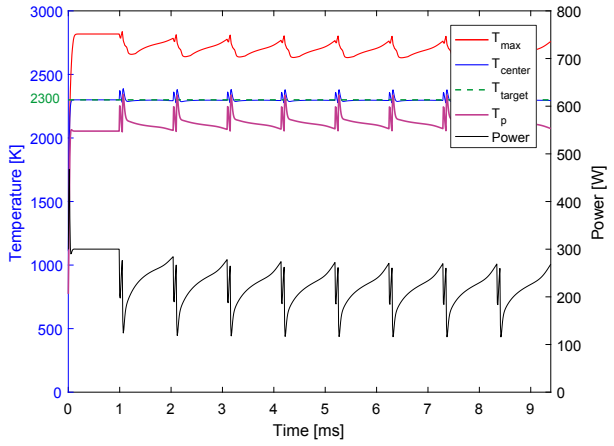

Figure 17: Evolution of temperatures and power over time with power modulation and continuous zigzag path

4 Conclusion

This paper presents a method to control the maximum temperature reached in a layer by modulating the laser power in LPBF. It takes advantage of a thermal model which allows a non-iterative calculation. The proposed approach consists in the evaluation of the required energy and thus lower power to adjust the

temperature at the center of the laser beam throughout the path. The various test cases in the case of Ti6Al4V highlight the efficiency of the method to control the temperature and homogenize the thermal distribution. As thermal gradients are lowered, residual stresses decrease too. In addition, the power modulation reduces the fluctuations of the melt pool size during the manufacturing process, thus reducing the defects generated by melting instability. The proposed method takes into account the kinematic behavior of the galvanometers in the scanning head, the technological constraints in the power calculation such as the response time of the laser as well as process constraints such as the process window specific to the material. The results have been validated numerically based on data from the recognized and commonly used literature. The experimental validation of the power modulation approach on an industrial machine is under investigation. Moreover, the temperature control by means of scanning speed modulation and modification of the scanning path geometry is part of the perspectives of this work.

5 Acknowledgments

This work is supported by the SOFIA project and funded by Bpifrance.

References

Béraud, N., Vignat, F., Villeneuve, F. and Dendievel, R. (2014), "New trajectories in Electron Beam Melting Manufacturing to reduce curling effect", *Procedia CIRP* Vol. 17, pp. 738-743, doi:10.1016/j.procir.2014.02.038.

Bertoli, U. S., Wolfer, A. J., Matthews, M. J., Delplanque, J. P. R. and Schoennung, J. M. (2016), "On the limitations of Volumetric Energy Density as a design parameter for Selective Laser Melting", *Materials & Design* Vol. 113, pp. 331-340, doi:10.1016/j.matdes.2016.10.037

Cernuschi, F., Russ, A. and Lorenzoni, L. (2001), "In-plane thermal diffusivity evaluation by infrared thermography", *Journal of Applied Physics* Vol. 72 No. 10, pp. 3988-3995, doi:10.1063/1.1400151.

Coeck, S., Bisht, M., Plas, J. and Verbist, F. (2019), "Prediction of lack of fusion porosity in selective laser melting based on melt pool monitoring data", *Additive Manufacturing* Vol. 25, pp. 347-356, doi:10.1016/j.addma.2018.11.015.

Dai, D. and Gu, D. (2015), "Tailoring surface quality through mass and momentumtransfer modeling using a volume of fluid method in selective laser melting of TiC/AlSi10Mg powder", *International Journal of Machine Tools and Manufacture*, Vol. 88, pp. 95-107, doi:10.1016/j.ijmachtools.2014.09.010.

Ettaieb, K., Lavernhe, S. and Tournier, C. (2020), "Fast thermal simulation of scanning paths in LPBF additive manufacturing", *Rapid Prototyping Journal*. Vol. 27 No. 4: pp. 720-734, doi:10.1108/RPJ-04-2020-0086

Forslund, R., Snis, A. and Larsson, S. (2019), "Analytical solution for heat conduction due to a moving Gaussian heat flux with piecewise constant parameters", *Applied Mathematical Modelling*, Vol. 12, pp. 227-240, doi:10.1016/j.apm.2018.09.018.

Forslund, R., Snis, A. and Larsson, S. (2021), "A greedy algorithm for optimal heating in powder-bed-based additive manufacturing", *Journal of Mathematics in Industry*, Vol. 11, No. 14, doi:10.1186/s13362-021-00110-x

Godineau, K., Lavernhe, S. and Tournier, C. (2019), "Calibration of galvanometric scan heads for additive manufacturing with machine assembly defects consideration", *Additive Manufacturing* Vol. 26, pp. 250-257, doi: 10.1016/j.addma.2019.02.003

Gong, H., Gu, H., Zeng, K., Dilip, J. J. S., Pal, D., Stucker, B., Christiansen, D., Beuth, J. and Lewandowski, J. J. (2014), "Melt Pool Characterization for Selective Laser Melting of Ti-6Al-4V Pre-alloyed Powder", *Conference: 25th Annual International Solid Freeform Fabrication Symposium* 12: pp. 256-267.

Gong, H., Rafi, K., GU, H., Janaki Ram, G. D., Starr, T. and Stucker, B. (2015), "Influence of defects on mechanical properties of Ti6Al4V components produced by selective laser melting and electron beam melting", *Materials & Design* Vol. 86, pp. 545-554, doi:10.1016/j.matdes.2015.07.147.

Kruth, J. P., Mercelis, P., Van vaerenbergh, J. and Craeghs, T. (2007), "Feedback control of selective laser melting", *3rd International Conference on Advanced Research in Virtual and Rapid Prototyping* pp. 521-527.

Kushan, M. C., Poyraz, O., Uzunonat, Y. and Orak, S. (2018), "Systematical review on the numerical simulations of laser powder bed additive manufacturing", *Sigma Journal of Engineering and Natural Sciences* Vol. 36 No. 4, pp. 1197-1214.

Lane, B., Mekhontsev, S., Grantham, S., Vlasea, M., Whiting, J., Yeung, H., Fox, J., Zarobila, C., Neira, J., McGlauflin, M. and Hanssen, L. (2016), "Design, developments, and results fromthe nist additive manufacturing metrology testbed (AMMT)", *Proceedings of the 26th Annual International Solid Freeform Fabrication Symposium An Additive Manufacturing Conference* pp. 1145-1160.

Mani, M., Donmez, M. A., Feng, S. C., Moylan, S., Fesperman, R. and Lane, B. (2015), "Measurement Science needs for real-time control of additive manufacturing Powder Bed Fusion Processes", *Technical report, National Institute of Standards and Technology, Gaithersburg, MD, NIST https://nvlpubs.nist.gov/nistpubs/ir/2015/NIST.IR.8036*.

Mugwagwa, L., Dimitrov, D. and Yadroitsev, I. (2018), "Influence of process parameters on residual stress related distortions in selective laser melting", *Procedia Manufacturing* Vol. 21, pp. 92-99, doi:10.1016/j.promfg.2018.02.099.

Muta, J., Nakata, S., Onda, T. and Chen, Z. C. (2018), "Optimization of selective laser melting parameters and influence of post heat treatment on microstructure and mechanical properties of maraging steel", textitProcedia Manufacturing Vol. 13, pp. 486-497, doi:10.1016/j.matdes.2017.11.042.

Nakapkin, D. S., Zakirov, A., Belousov, S., Bogdanova, M., Korneev, B., Stepanov, A., Perepelkina, A., Levchenko, V., Potapkin, B. and Meshkov, A. (2019), "Finding optimal parameter ranges for laser powder bed fusion with predictive modeling at mesoscale", *II International Conference on Simulation for Additive Manufacturing-Sim-AM 2019, Pavia, Italy* Vol. 12: pp. 297-308.

Oliveira, J. P., Lalonde, A. D., Ma, J. (2020), "Processing parameters in laser powder bed fusion metal additive manufacturing." *Materials & Design* Vol. 12 No. 193, 108762, doi:10.1016/j.matdes.2020.108762

Tapia, G. and Elwany, A. (2014), "A review on process monitoring and control in metal-based additive manufacturing", *Journal of Manufacturing Science and Engineering* Vol. 136 No. 6, 060801, doi:10.1115/1.4028540.

Thijs, L., Verhaeghe, F., Craeghs, T., Humbeeck, J. V. and Kruth, J. P. (2010), "A study of the microstructural evolution during selective laser melting of Ti6Al4V", *Acta Materialia* Vol. 58 No. 9, pp. 3303-3312, doi:10.1016/j.actamat.2010.02.004.

Yeung, H., Lane, B., Domnez, J., Fox, J. and Neira, J. (2018), "Implementation of advanced laser control strategies for powder bed fusion systems", *46th SME North American Manufacturing Research Conference, NAMRC 46, Texas, USA* Vol. 26, pp. 871-879, doi:10.1016/j.promfg.2018.07.112.

Yeung, H., Lane, B. and Fox, J. (2019), "Part geometry and conduction-based laser power control for powder bed fusion additive manufacturing", *Additive Manufacturing* Vol. 30, 100844, doi:10.1016/j.addma.2019.100844

Zhang, B., Li, Y. and Bai, Q. (2017), "Defect formation mechanisms in Selective Laser Melting: a review." *Chinese Journal of Mechanical Engineering*, Vol. 30 No. 3, pp. 515-527, doi:10.1007/s10033-017-0121-5.